1996AJ....111.1356D

THE ASTRONOMICAL JOURNAL VOLUME 111, NUMBER 3 MARCH 1996

MULTIWAVELENGTH OBSERVATIONS OF TWO MODERATE ROTATION RS CVn SYSTEMS: V815 HERCULIS AND IM PEGASI

ROBERT C. DEMPSEY[1,2]

Astronomy Programs, Computer Sciences Corporation, Space Telescope Science Institute, 3700 San Martin Drive, Baltimore, Maryland 21218
Electronic mail: dempsey@stsci.edu

JAMES E. NEFF[2,3] AND DOUGLAS O'NEAL

The Pennsylvania State University, Department of Astronomy and Astrophysics, 525 Davey Lab, University Park, Pennsylvania 16802

KATALIN OLAH

Konkoly Observatory, P.O. Box 67, 1525 Budapest, Hungary

Received 1995 April 18; revised 1995 November 21

ABSTRACT

Near-to-simultaneous ultraviolet and visual spectroscopy of two moderate $v \sin i$ RS CVn systems, V815 Herculis ($v \sin i = 27$ km s^{-1}) and IM Pegasi ($v \sin i = 24$ km s^{-1}), are presented along with contemporaneous $UBV(RI)_c$ photometry. These data were used to probe inhomogeneities in the chromospheres and photospheres, and the possible relationship between them. Variability is observed at all wavelengths, some indicators showing rotationally modulated fluctuations. We use *UBVRI* photometry and TiO spectra to estimate temperatures, area, and locations of photospheric spots on IM Peg. Evidence is presented that the spot temperature in IM Peg has changed over a possible solar-like spot cycle. Radial velocities of V815 Her indicates that the system is actually triple. © *1996 American Astronomical Society.*

1. INTRODUCTION

A very extensive literature details variability of late-type stars in different transitions such as Ca II H and K, Hα, C IV, Mg II, and in radio and x-ray wavelength regions. Variation in the emission in these lines is usually taken as an indication of inhomogeneities in the chromosphere, transition region (TR), or corona. Such emission fluctuations are usually accompanied by visual *UBV*-band modulation that is generally believed to be the result of large, cool regions located in the photosphere, similar to sunspots. In some studies the chromospheric emission varies in antiphase with the photometric wave (increased emission at photometric minimum), which suggests that the active regions are compact and cospatial with spots (e.g., Rodonò *et al.* 1987; Huenemoerder *et al.* 1990; Dempsey *et al.* 1993a). Just as frequently, however, no correlation or a very complex correlation is observed (e.g., Doyle *et al.* 1989). Ideally, simultaneous observations should be performed at all wavelengths in order to develop a coherent 3D atmosphere model. In practice, observations of several proxy indicators simultaneously are rare and tend to focus on the same small number of extremely active systems. Dominating such studies are the RS Canum Venaticorum (RS CVn) and BY Draconis (BY Dra) binaries. The RS CVn systems, first identified by Hall (1976), typically consist of a G- or K-type giant or subgiant with a late-type main sequence or subgiant companion. BY Draconis (BY Dra) binaries contain two late-type main-sequence stars. We have been conducting a campaign to probe surface inhomogeneities on a large number of systems, many with moderate to low levels of activity (Dempsey *et al.* 1992; 1993a).

In this paper we present near-to-simultaneous visual and ultraviolet observations of two active binaries with very different periods. The first system, V815 Herculis (HD 166181), consists of a G5 V star whose rotation rate is tidally locked with its 1.8 day orbit with an M1−2V companion. Spots are clearly indicated in visual photometric light curves, which typically show a modulation of $0^m.13$. Dempsey *et al.* (1993b) found the system to be x-ray luminous. An x-ray flare has been observed on the system as well as a possible modulation of the x-ray emission due to stellar rotation (Dempsey *et al.* 1993c; Dempsey *et al.* 1995). Although it is likely that the spot wave of the visual light curve results from an inhomogeneous photosphere on the G5 V star, the observed x-ray flare could have occurred on either component.

The second, better studied system, IM Pegasi (HD 216489), contains a K2 III-II primary plus an unknown companion and has an orbital period of 24 days. Dempsey *et al.*

[1]Visiting Astronomer, Kitt Peak National Observatory, National Optical Astronomy Observatories, which is operated by AURA, Inc. under cooperative agreement with the National Science Foundation.
[2]Guest Investigator with the International Ultraviolet Explorer satellite, which is sponsored and operated by the National Aeronautics and Space Administration, by the the Science Research Council of the United Kingdom, and by the European Space Agency.
[3]Visiting Astronomer, National Solar Observatory, National Optical Astronomy Observatories, which is operated by AURA, Inc. under cooperative agreement with the National Science Foundation.

 0004-6256/96/111(3)/1356/12/$6.00 © 1996 Am. Astron. Soc.

© American Astronomical Society • Provided by the NASA Astrophysics Data System

1996AJ....111.1356D

TABLE 1. Log of visual observations.

Target	UT Date	Exposure (sec)	UT Start	Phase	Region	Observatory[a]
IM Peg	02-aug-1992	900	07:17	0.89	echelle	BMO
IM Peg	03-aug-1992	900	07:02	0.93	echelle	BMO
IM Peg	05-aug-1992	900	06:51	0.01	echelle	BMO
IM Peg	06-aug-1992	600	06:52	0.05	echelle	BMO
IM Peg	07-aug-1992	900	06:33	0.09	echelle	BMO
IM Peg	12-aug-1992	900	05:22	0.29	echelle	BMO
IM Peg	20-aug-1992	900	04:27	0.61	echelle	BMO
V815 Her	11-sep-1992	1800	02:49	0.99	Hα	NSO
IM Peg		900	04:06	0.50	Hα	NSO
IM Peg		900	06:14	0.50	He I	NSO
IM Peg		600	08:12	0.50	Hβ	NSO
IM Peg		129	09:52	0.50	TiO-7100	NSO
IM Peg		480	10:45	0.50	TiO-8860	NSO
IM Peg	12-sep-1992	540	03:45	0.55	TiO-8860	NSO
IM Peg		120	05:49	0.55	TiO-7100	NSO
IM Peg		600	07:16	0.55	Hα	NSO
IM Peg		360	09:26	0.55	He I	NSO
IM Peg		600	10:54	0.55	Hβ	NSO
IM Peg	14-sep-1992	600	04:53	0.63	TiO-8860	NSO
IM Peg		120	07:02	0.63	TiO-7100	NSO
IM Peg		420	07:25	0.63	Hα	NSO
IM Peg		300	10:25	0.63	He I	NSO
IM Peg		600	11:07	0.63	Hβ	NSO
IM Peg	15-sep-1992	120	03:52	0.67	TiO-7100	NSO
IM Peg		540	06:00	0.67	TiO-8860	NSO
IM Peg		420	07:53	0.67	Hα	NSO
IM Peg		600	09:30	0.67	He I	NSO
IM Peg	16-sep-1992	480	08:14	0.71	Hα	NSO
V815 Her	22-sep-1992	2000	02:16	0.06	6420	CF
IM Peg		600	04:05	0.96	6420	CF
V815 Her		1800	04:38	0.11	6420	CF
V815 Her		1800	05:28	0.13	IRT	CF
IM Peg		2700	06:56	0.96	IRT	CF
IM Peg		300	09:24	0.96	Hα	CF
V815 Her	23-sep-1992	1800	02:18	0.61	IRT	CF
V815 Her		2100	02:58	0.63	6420	CF
IM Peg		300	06:39	1.00	Hα	CF
IM Peg		1200	07:41	1.00	IRT	CF
V815 Her	24-sep-1992	2100	02:09	0.16	IRT	CF
V815 Her		2000	03:50	0.20	6420	CF
V815 Her		900	04:50	0.22	Hα	CF
IM Peg		300	05:38	0.03	Hα	CF
IM Peg		300	06:46	0.03	6420	CF
V815 Her	25-sep-1992	2100	02:15	0.72	IRT	CF
V815 Her		2000	03:50	0.75	6420	CF
V815 Her		900	04:50	0.77	Hα	CF
IM Peg		300	05:44	0.08	Hα	CF
IM Peg		300	06:50	0.08	6420	CF
IM Peg		1200	07:51	0.08	IRT	CF
V815 Her	26-sep-1992	2100	02:09	0.27	IRT	CF
V815 Her		2100	02:48	0.28	IRT	CF
V815 Her		2000	03:29	0.30	6420	CF
V815 Her		1000	05:25	0.34	Hα	CF
IM Peg		300	06:06	0.11	Hα	CF
IM Peg		1200	06:49	0.11	IRT	CF
IM Peg		300	08:12	0.11	6420	CF
V815 Her	27-sep-1992	2000	02:04	0.82	IRT	CF
V815 Her		2000	03:48	0.86	6420	CF
V815 Her		1000	05:24	0.89	Hα	CF
IM Peg		300	06:04	0.16	Hα	CF
V815 Her	28-sep-1992	1800	02:34	0.38	IRT	CF
V815 Her		2000	03:58	0.41	6420	CF
V815 Her		900	04:55	0.43	Hα	CF
IM Peg		300	05:30	0.20	Hα	CF
IM Peg		1500	06:43	0.20	IRT	CF
IM Peg		400	08:10	0.20	6420	CF
IM Peg	14-oct-1992	450	02:34	0.84	echelle	BMO
IM Peg	22-oct-1992	3000	02:20	0.16	Hα	RO
IM Peg	25-oct-1992	2500	01:24	0.29	Hα	RO
IM Peg	26-oct-1992	2500	01:30	0.33	Hα	RO
IM Peg	27-oct-1992	450	02:07	0.37	echelle	BMO
IM Peg		1200	02:45	0.37	echelle	BMO
IM Peg		450	02:07	0.37	echelle	BMO
IM Peg	28-oct-1992	600	02:19	0.41	echelle	BMO
IM Peg		600	02:31	0.41	echelle	BMO
IM Peg		600	02:41	0.41	echelle	BMO
IM Peg		600	02:51	0.41	echelle	BMO
IM Peg	29-oct-1992	600	01:42	0.45	echelle	BMO
IM Peg		600	01:53	0.45	echelle	BMO
IM Peg		600	02:03	0.45	echelle	BMO
IM Peg		600	02:14	0.45	echelle	BMO
IM Peg	08-nov-1992	420	02:50	0.86	echelle	BMO
IM Peg		420	02:57	0.86	echelle	BMO
IM Peg		420	03:05	0.86	echelle	BMO

[a]Symbol indicates where data were obtained: NSO=National Solar Observatory's McMath-Pierce telescope and stellar spectrograph, CF=Kitt Peak National Observatory's coudé feed telescope, RO=the University of Toledo's Ritter Observatory, and BMO=Penn State University's 1.6 m telescope and echelle spectrograph at Black Moshannon Observatory.

(1994) studied spectral line profile variations in this system and concluded that high-latitude, but not polar, spots were present. IM Peg also exhibits rotational modulation of the Ca II infrared "triplet" (IRT) and Hα emission (Huenemoerder *et al.* 1990; Dempsey *et al.* 1993a). Although bright in x rays, $L_X \sim 5.3\times10^{30}$ ergs s^{-1}, no coronal inhomogeneities were detected during the *ROSAT* All-Sky Survey (Dempsey *et al.* 1993b, 1995). IM Peg has now been observed in the visual by us over many years. Dempsey *et al.* (1994) presented preliminary results that IM Peg appears to show a solar-like spot cycle with a period of 12–15 years. Results from the multiyear spot modelling will be presented in full in a later publication.

2. OBSERVATIONS

2.1 Visual Spectroscopic Data

Spectroscopic observations for V815 Her and IM Peg were obtained in September 1992 from Kitt Peak National Observatory (KPNO) using the coudé feed telescope. The 1024×1024 TIKA CCD (27 μ pixels) was used with grating A, camera 5, and the long collimator resulting in a two-pixel resolution of 0.32 Å at 6400 Å. Spectra covered Hα, the 8498 and 8542 lines of the IRT, and the 6390–6430 Å region. Additional data for IM Peg were obtained with the National Solar Observatory (NSO). The NSO observations used the Milton-Roy grating #1 (1200 lines/mm) in second order with an 800×800 TI CCD (15 μm pixels) and have a two-pixel resolution of 0.19 Å at Hα. Several spectra of the Hα region with a resolution of 0.11 Å were obtained with the Ritter Observatory (RO) 1 m telescope employing a fiber-fed echelle (see Dempsey *et al.* 1992 for details). Low-resolution (Δλ 1.24–2.26 Å) echelle observations covering essentially all of the 4400–9000 Å region were obtained at the Black Moshannon Observatory (BMO). Spectra obtained at NSO and BMO covered the Na I D and He I D_3 lines, Hα, Hβ, and two titanium oxide (TiO) bands. The KPNO and RO data

© American Astronomical Society • Provided by the NASA Astrophysics Data System

1996AJ....111.1356D

TABLE 2. V815 Her photometry obtained at Konkoly Observatory.

HJD (+2440000)	Phase	ΔV[a]	$(U-B)$	$(B-V)$	$(V-I)$	$(V-R)$
8748.4219	0.15	0.863	0.103	0.079	0.174	0.079
8798.4414	0.79	0.859	0.094	0.080	0.165	0.068
8800.4141	0.88	0.882	0.089	0.085	0.181	0.078
8801.4102	0.43	0.855	0.092	0.077	0.172	0.074
8802.5469	0.06	0.875	0.089	0.081	0.173	0.076
8803.5391	0.61	0.841	0.104	0.080	0.162	0.074
8804.4609	0.12	0.866	0.097	0.079	0.176	0.077
8805.4062	0.64	0.832	0.093	0.081	0.168	0.071
8808.5391	0.37	0.872	0.087	0.079	0.176	0.077
8859.3555	0.45	0.868	0.086	0.089	0.175	0.079
8860.3789	0.01	0.867	0.090	0.084	0.173	0.067
8861.3789	0.57	0.875	0.087	0.079	0.169	0.073
8883.3633	0.71	0.835	0.090	0.071	0.165	0.070
8884.2617	0.21	0.854	0.088	0.077	0.170	0.074
8885.2734	0.77	0.851	0.091	0.079	0.169	0.073
8886.2734	0.32	0.838	0.080	0.076	0.167	0.070
8888.2539	0.42	0.837	0.084	0.081	0.158	0.066
8888.2812	0.43	0.836	0.086	0.074	0.159	0.071
8890.3516	0.58	0.837	0.076	0.078	0.160	0.071
8891.2461	0.07	0.890	0.096	0.084	0.182	0.074
8892.2500	0.62	0.840	0.080	0.078	0.165	0.070
Mean		0.856	0.900	0.080	0.170	0.073
σ[b]		0.078	0.032	0.018	0.027	0.018

Notes to TABLE 2

[a]Differential photometry relative to BD+29° 3190 (V=6.85, $U-B$=0.22, $B-V$=0.64, $V-R_c$=0.34, $V-I_c$=0.71.
[b]Standard deviation.

TABLE 3. IM Peg photometry obtained at Konkoly Observatory

HJD (+2440000)	Phase	ΔV[a]	$(U-B)$	$(B-V)$	$(V-I)$	$(V-R)$
8859.4453	0.80	-0.795	0.204	0.131	0.116	0.086
8860.6016	0.85	-0.792	0.192	0.124	0.117	0.084
8862.5625	0.93	-0.759	0.196	0.136	0.132	0.090
8863.5703	0.97	-0.732	0.200	0.140	0.133	0.097
8883.5000	0.78	-0.779	0.207	0.123	0.127	0.091
8886.3906	0.90	-0.765	0.204	0.132	0.135	0.095
8888.4336	0.98	-0.730	0.212	0.143	0.142	0.095
8890.4258	0.06	-0.701	0.202	0.143	0.146	0.098
8891.3789	0.10	-0.701	0.205	0.149	0.154	0.099
8892.5273	0.15	-0.693	0.206	0.138	0.150	0.098
8897.4102	0.34	-0.705	0.206	0.132	0.152	0.095
8954.1953	0.65	-0.701	0.215	0.136	0.158	0.106
8954.3164	0.65	-0.689	0.213	0.126	0.159	0.103
8956.1914	0.73	-0.757	0.211	0.128	0.133	0.090
8957.3242	0.78	-0.780	0.203	0.128	0.127	0.089
8974.2773	0.46	-0.666	0.208	0.133	0.164	0.109
8975.1875	0.50	-0.659	0.199	0.142	0.164	0.101
8979.1680	0.66	-0.715	0.202	0.143	0.153	0.094
Mean		-0.729	0.205	0.135	0.142	0.096
σ[b]		0.178	0.025	0.030	0.064	0.025

Notes to TABLE 3

[a]Differential photometry relative to HD 216635 (V=6.617, $U-B$=0.74, $B-V$=1.04, $V-R_c$=0.555, $V-I_c$=1.053.)
[b]Standard Deviation.

were reduced in a standard fashion using IRAF.[4] The NSO data reduction followed the procedures outlined in Neff *et al.* (1995), using IDL routines developed in house but made publicly available. The BMO data reduction used the IDL-based echelle reduction package described by Hall *et al.* (1994). Signal-to-noise was typically 150–200 for the KPNO 6400 Å region and 60–100 for the other wavelength regions. For the RO spectra S/N was typically 35–80. For the BMO data S/N was usually 100–125. A log of the visual spectroscopic observations is given in Table 1.

Due to the $v \sin i$ and lower activity levels of the stars studied here, measuring small changes in the line core emission is difficult. For example, equivalent widths usually have large errors due to uncertainties in continuum placement, definition of the line wings, line blends including those of the secondary, and artifacts such as water vapor lines (Bopp *et al.* 1988). Subtraction of an "inactive" star requires high S/N spectra of stars with identical properties. Instead, we measure the residual line core intensity, R_c. Bopp *et al.* (1988), Dempsey (1991), Dempsey *et al.* (1993a), and Montes *et al.* (1995) showed how R_c can accurately measure small changes in chromospheric emission of Hα and the IRT. For both systems discussed here, the IRT lines usually have an emission reversal in the high-resolution spectra. In these cases, R_c is the intensity of the core emission peak divided by the continuum intensity. For the lower-resolution BMO data the emission reversal is generally not resolved, so R_C represents the lowest point in the absorption line. Phases for V815 Her were computed from the ephemeris HJD 2441930.4877+1.8098368E (Strassmeier *et al.* 1993) and for IM Peg using HJD 2422243.316+24.649E (Eaton *et al.* 1983).

2.2 Visual Photometric Data

At Konkoly Observatory $UBV(RI)_C$ photometric observations were made in 1992 for both systems in May through September for V815 Her and from August to December for IM Peg using the 1 m RCC telescope. These data are listed in Tables 2 and 3. Average first- and second-order extinction coefficients were used. First-order standards are from Landolt (1983) with standard magnitudes recalibrated by Menzies *et al.* (1991). Each data value is actually an average of several observations, usually 6, with standard deviations typically of 0.003–0.004.

2.3 Ultraviolet Spectroscopic Data

Ultraviolet spectra were obtained with the *International Ultraviolet Explorer* (*IUE*) during the fall of 1992. The *IUE* observation log is given in Table 4. Both SWP low-resolution and LWP high-resolution spectra were obtained at a number of phases that were intended to evenly cover one rotation cycle of the systems. For V815 Her the spectra were obtained over 15 days, overlapping with the ground-based KPNO observations. *IUE* spectra for IM Peg were obtained over a 17 day interval and partially overlapped the visual observations.

Spectra were extracted and calibrated from the *IUE* images with the RDAF package of IDL routines. Line fluxes

[4]IRAF is distributed by National Optical Astronomy Observatories, which is operated by the Association of Universities for Research in Astronomy, Inc., under contract with the National Science Foundation.

© American Astronomical Society • Provided by the NASA Astrophysics Data System

1996AJ....111.1356D

TABLE 4. Log of IUE observations.

Image	Target	UT Exposure Start	Duration (sec)	Phase (Start)
LWP 23976	V815 Her	20-sep-1992 03:46:12	1800.000	0.26
SWP 45689	V815 Her	20-sep-1992 04:23:17	9000.000	0.30
LWP 23980	V815 Her	22-sep-1992 03:54:57	1800.000	1.37
SWP 45740	V815 Her	22-sep-1992 04:33:01	8400.000	1.41
LWP 23988	V815 Her	23-sep-1992 03:05:24	1800.000	1.90
SWP 45752	V815 Her	23-sep-1992 03:40:18	11100.000	1.95
LWP 23993	V815 Her	24-sep-1992 03:36:12	1800.000	2.47
SWP 45764	V815 Her	24-sep-1992 04:11:28	9600.000	2.51
LWP 24000	V815 Her	25-sep-1992 03:31:55	1800.000	3.02
SWP 45768	V815 Her	25-sep-1992 04:07:28	9720.000	3.06
LWP 24005	V815 Her	26-sep-1992 03:43:53	1800.000	3.58
SWP 45775	V815 Her	26-sep-1992 04:18:55	9000.000	3.61
LWP 24010	V815 Her	27-sep-1992 03:45:47	1800.000	4.13
SWP 45782	V815 Her	27-sep-1992 04:20:34	9000.000	4.17
LWP 24018	V815 Her	28-sep-1992 03:33:04	1800.000	4.68
SWP 45785	V815 Her	28-sep-1992 04:08:10	9823.000	4.72
LWP 24075	V815 Her	05-oct-1992 01:40:06	1800.000	8.50
SWP 45842	V815 Her	05-oct-1992 02:14:55	9300.000	8.54
LWP 24134	IM Peg	22-oct-1992 10:18:55	1800.000	0.18
SWP 46035	IM Peg	22-oct-1992 10:55:28	5400.000	0.18
LWP 24135	IM Peg	22-oct-1992 12:31:53	1080.000	0.18
LWP 24141	IM Peg	24-oct-1992 10:09:10	1800.000	0.26
SWP 46049	IM Peg	24-oct-1992 10:45:02	5400.000	0.26
LWP 24142	IM Peg	24-oct-1992 12:26:56	1200.000	0.26
LWP 24156	IM Peg	26-oct-1992 09:35:08	1800.000	0.34
SWP 46066	IM Peg	26-oct-1992 10:13:18	5400.000	0.34
LWP 24157	IM Peg	26-oct-1992 11:47:56	1200.000	0.34
SWP 46067	IM Peg	26-oct-1992 12:19:11	1800.000	0.34
LWP 24171	IM Peg	28-oct-1992 10:00:28	1800.000	0.42
SWP 46084	IM Peg	28-oct-1992 10:38:38	6600.000	0.42
LWP 24172	IM Peg	28-oct-1992 12:33:32	960.000	0.42
LWP 24193	IM Peg	30-oct-1992 09:31:21	1800.000	0.50
SWP 46098	IM Peg	30-oct-1992 10:14:19	6600.000	0.50
LWP 24194	IM Peg	30-oct-1992 12:13:03	1200.000	0.50
SWP 46120	IM Peg	03-nov-1992 07:44:52	6600.000	0.66
LWP 24249	IM Peg	03-nov-1992 07:19:52	1200.000	0.66
LWP 24250	IM Peg	03-nov-1992 09:45:00	1500.000	0.66
LWP 24290	IM Peg	07-nov-1992 07:59:00	1500.000	0.82
SWP 46150	IM Peg	07-nov-1992 08:29:47	6600.000	0.82
LWP 24291	IM Peg	07-nov-1992 10:29:10	1200.000	0.83

were measured by fitting the line profiles using the ICUR fitting code based on Bevington's (1969) CURFIT (Neff 1987). The emission lines were modeled as Gaussian in shape, and the background is extrapolated from a quadratic fit to the region on both sides of the line. Up to five Gaussians can be fit simultaneously, permitting us to resolve the individual contributions of blended lines. Further details on the fitting may be found in Neff *et al.* (1989).

The uncertainty in the absolute flux scale for *IUE* is generally 15%–20%, but we are interested here primarily in relative fluxes measured at the same epoch with the same procedure. We first performed a series of repeated measurements of the same line using different input parameters. The scatter in these measurements was ±5%–10% (cf. Bohlin 1986; Bohlin & Grillmair 1987; Linsky *et al.* 1989; Ayres *et al.* 1995). Using a consistent set of input parameters for any given line leads to less scatter. To quantify this, we used the average residuals between the data and our background fits to determine a minimum detectable flux for each line and

TABLE 5. V815 Her radial velocities

HJD	Phase	RV km s^{-1}	Weight	O–C km s^{-1}
2432760.6650	0.169	−44.20	0.8	0.18
2433136.5870	0.880	−19.10	0.8	−0.25
2433507.6530	0.907	−20.60	0.8	7.48
2433772.8750	0.452	42.90	0.8	4.86
2434303.5210	0.653	41.50	0.8	-4.92
2441480.5790	0.239	-11.80	0.8	13.41
2441488.5390	0.637	50.70	0.8	2.29
2441812.5380	0.658	45.20	0.8	-0.45
2441864.4600	0.347	7.80	0.8	-2.11
2441865.4540	0.896	-23.00	0.8	1.59
2441866.5030	0.476	41.60	0.8	-1.05
2441867.4550	0.002	-49.10	0.8	2.75
2441868.5410	0.602	53.70	0.8	2.56
2441869.5570	0.164	-49.80	0.8	-4.20
2441870.4800	0.674	42.70	0.8	-0.51
2441930.3330	0.744	20.70	0.8	-5.98
2441930.4880	0.830	1.20	0.8	2.55
2441931.3220	0.291	-14.20	0.8	-5.78
2441932.3370	0.852	-9.40	0.8	-0.35
2441933.3340	0.403	23.40	0.8	-2.81
2441934.3280	0.952	-45.40	0.8	-4.14
2441935.4240	0.557	50.10	0.8	-1.24
2441936.3400	0.064	-58.60	0.8	-1.73
2448678.9941	0.625	52.20	1.0	2.62
2448679.9753	0.168	-42.20	1.0	2.50
2448681.0076	0.738	31.80	1.0	3.30
2448681.9170	0.240	-23.40	1.0	1.36
2448887.6062	0.891	-26.50	1.0	-3.67
2448888.6359	0.460	36.40	1.0	-3.31
2448889.6713	0.032	-55.70	1.0	-0.21
2448889.7066	0.052	-57.20	1.0	-0.56
2448890.6713	0.585	52.30	1.0	0.64
2448890.7066	0.604	54.70	1.0	3.66
2448891.6566	0.129	-53.80	1.0	-1.86
2448892.6698	0.689	36.40	1.0	-3.87
2448893.6767	0.245	-27.20	1.0	-3.99

added this constant to the flux uncertainty returned with each Gaussian line fit. This provides a more realistic uncertainty for the weak lines, because the uncertainties in the flux measurements are generally only 1%–3%. The final error bars shown in the figures provide our best estimate of the reproducibility of our flux measurements when they are measured assuming a systematic background definition. Several sources of nonrandom errors, such as fixed-pattern noise, are introduced in the detector and in the calibration software. These will be better quantified in the final processing software. We have not included an explicit correction for nonrandom errors in the final extracted spectra. They could affect individual points but are unlikely to mimic rotational modulation.

3. V815 Her

3.1 Orbit

While measuring wavelengths of some of the visual lines it became apparent that the orbit presented in Nadal *et al.* (1974) did not accurately predict line positions for our data. We therefore measured 13 radial velocities from the KPNO spectra using the cross-correlation method discussed in Bopp

© American Astronomical Society • Provided by the NASA Astrophysics Data System

1996AJ....111.1356D

TABLE 6. Orbital solutions

Dataset	γ km s^{-1}	K km s^{-1}	e	ω deg	T_o	P_{orb} days
Nadal et al.	−12.4	53.7	0.05	167.1	2,441,930.86	1.8098352
±	1.1	1.6	0.03	33.5	0.17	0.0000040
KPNO	−1.6	54.9	0.05	103.2	2,441,926.80	1.8098664
±	1.0	1.2	0.02	28.9	0.56	0.0001400

& Dempsey (1989). For the cross correlations we used the 6390–6430 Å and 6570–6590 Å regions. For the standard star we used μ Her (G5 IV) with a radial velocity of −15.9 km s^{-1}. In several cases we also used β Com (G0 V, +6.0 km s^{-1}) as a check star. Velocities using both standard stars agreed to better than 0.3 km s^{-1}. Results are listed in Table 5. We estimate the errors of the new velocities to be better than 1 km s^{-1} at the spectral resolution and S/N of our data (Bopp & Dempsey 1989). Overplotting the new data with those from Nadal *et al.* clearly showed that a systematic shift of approximately 12 km s^{-1} existed between the two sets of radial velocities. To accurately estimate the shift, we calculated the orbit for both the old and new data sets using the standard least-squares program of Bopp *et al.* (1970). From the data of Nadal *et al.* we find a center of mass velocity γ of −12.4±1.1 km s^{-1}, compared to −1.6±1.0 km s^{-1} for the KPNO observations. Except for γ all new orbital elements were within errors to the published orbit (see Table 6). Phasing all the data gives an improved period of P_{rot}=1^d.8098355±0.0000021. The final orbit is shown in Fig. 1.

While a systematic error in the velocities of Nadal *et al.* is possible (e.g., Bopp *et al.* 1989), such a large offset would be unlikely. A more plausible possibility is that an undetected third body is present in the V815 Her system with an orbital period of many years. The only apparent effect of the third body is to change γ and not any of the other orbital elements.

3.2 Visual Data

No line profile shape variations were detectable for V815 Her at this spectral resolution and signal-to-noise. An emission reversal is visible in the IRT lines (Fig. 2). The level of activity shown at the IRT is consistent with other active stars with similar periods and spectral types (Dempsey *et al.* 1993a). Emission filling in the line core of Hα (Fig. 3) is also evident (for comparison see Bopp *et al.* 1988; Dempsey 1991). Measurements of R_c (Table 7) show substantial variability of the IRT and Hα line core emission, but none that is clearly in phase with the rotational period. The uncertainty of a single R_c is estimated from repeated measurements to be approximately 0.002 for the higher resolution data and 0.003 for the BMO spectra. At this resolution, an inactive star typically has a seasonal standard deviation around 0.004−0.007 (Bopp *et al.* 1988).

Photometry for V815 Her are shown in Fig. 4. Unfortunately, few data points are available in late September when the *IUE* and KPNO observations were obtained, but a minimum is apparent around phase 0.0 followed by a steep rise to maximum around phase 0.3. The light level is roughly constant until phase 0.8 where it may again decrease. The late

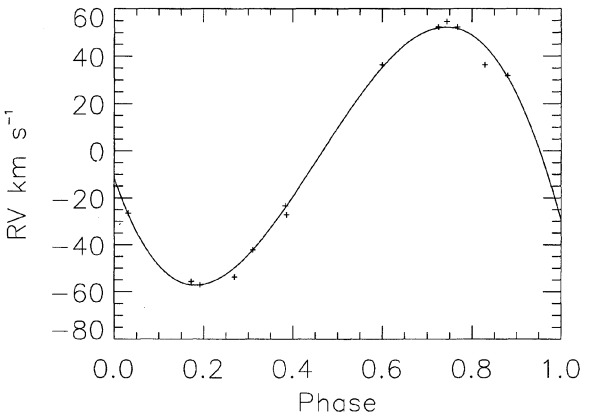

FIG. 1. Radial velocities for V815 Her with the derived KPNO orbital solution (solid line).

September light curve is noticeably different than the May–August light curve, indicating that the light curve for V815 Her changes shape dramatically in the interval of several weeks (≈10 stellar rotations).

3.3 Ultraviolet Data

An example of the LWP high-resolution Mg II spectrum for V815 Her is shown in Fig. 5. Phases of conjunction show a single strong Mg II H and K line. In several cases, especially at the quadrature phases, emission from both stellar components was resolved. A weak, unresolved interstellar line might be visible in several spectra, but this feature could not be reliably fit. The results of fitting a Gaussian emission line plus a quadratic background to each spectrum are listed in Table 8. Velocities for the stronger component correspond to the predicted position of the G star. We conclude that approximately 19% of the Mg II line flux comes from the M star.

A representative SWP spectrum of V815 Her is shown in Fig. 6. Because of the low (6 Å) resolution, only a single

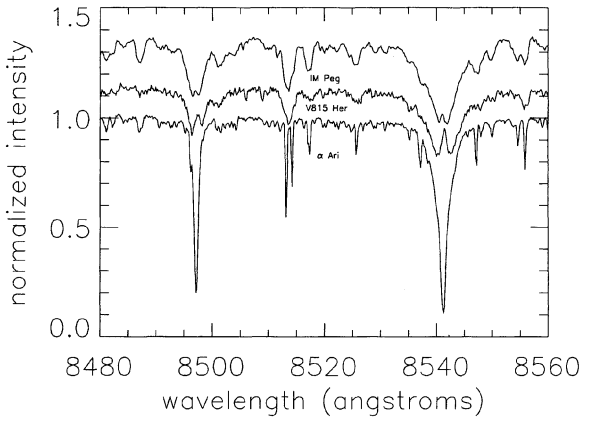

FIG. 2. Ca II infrared triplet (IRT) region of V815 Her (middle spectrum), IM Peg (top spectrum) and the standard star α Arietis (K2 III, bottom spectrum). Emission reversals are clearly seen in the λ 8498 and λ 8542 Ca II lines in both of the RS CVn spectra. Spectra have been normalized to unity and the upper two shifted arbitrarily in the vertical direction for clarity.

© American Astronomical Society • Provided by the NASA Astrophysics Data System

1996AJ....111.1356D

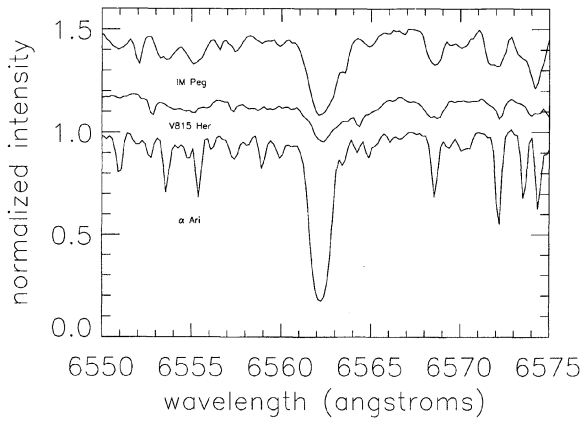

FIG. 3. H I Balmer-α region of V815 Her (middle spectrum), IM Peg (top), and α Ari (bottom). The shallowness of the Hα (6563 Å) line cores in V815 Her and IM Peg result from both rotational broadening and chromospheric emission. Spectra have been normalized to unity and the upper two shifted arbitrarily in the vertical direction for clarity.

component can be resolved, which contains contributions from both stars. Table 9 lists all the far-ultraviolet emission line fluxes measured by fitting Gaussian profiles and a quadratic background to the SWP spectra. In Fig. 7 we compare the transition region and chromospheric fluxes as a function of rotational phase.

4. IM Peg

4.1 Visual Data

A typical IRT spectrum of IM Peg is shown in Fig. 2. The activity level observed in September of 1992 was the same as that observed by Dempsey *et al.* (1993a). Variations in R_c for the Hα and IRT lines (see Table 10) are evident but subtle, as seen in Fig. 8. Contemporaneous light curves are shown in Fig. 9. The high-resolution Hα data, and to a lesser degree the λ8498 data, show a clear increase while the *V*-band light curve (see lower panel, Fig. 9) appears to decrease between phase 0.0 and 0.2. Around photometric maximum at phase 0.8 the Hα emission was at a minimum. The λ8542 data mimic those for λ8498 but with a smaller amplitude. Too few of the Hβ observations are available to draw any conclusions about variability. Thus IM Peg may exhibit an antiphase correlation between brightness and chromo-

TABLE 7. V815 Her R_c measurements.[a]

HJD (+2440000)	Phase	Hα	8498Å	8542Å	8662Å
8876.62	0.99	0.76	–	–	–
8887.74	0.13	–	0.84	0.78	–
8888.60	0.61	–	0.84	0.77	–
8889.60	0.16	–	0.87	0.82	–
8889.71	0.22	0.76	–	–	–
8890.61	0.72	–	0.88	0.80	–
8890.71	0.77	0.71	–	–	–
8891.60	0.27	–	0.86	0.76	–
8891.63	0.28	–	0.84	0.78	–
8891.73	0.34	0.71	–	–	–
8892.60	0.82	–	0.85	0.79	–
8892.73	0.89	0.68	–	–	–
8893.61	0.38	–	0.88	0.78	–
8893.71	0.43	0.75	–	–	–
Mean		0.73	0.865	0.78	
σ		0.03	0.02	0.02	

Note to TABLE 7

[a]Entries with "–" indicate no observation on that date for that wavelength.

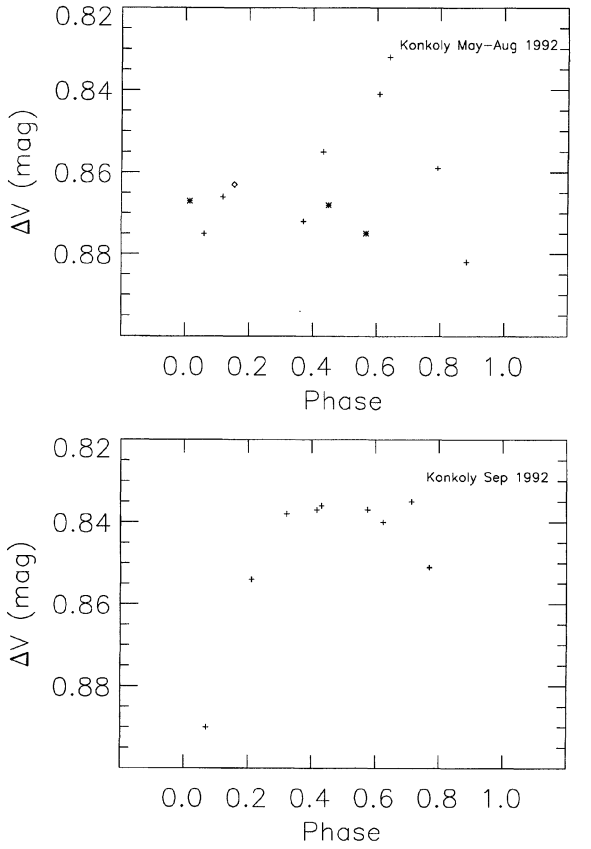

FIG. 4. *V*-band light curve for V815 Her from May through August (top) and for September when the *IUE* observations were obtained (bottom). In the top figure the diamond, pluses, and asterisks indicate data from May, June, and August, respectively.

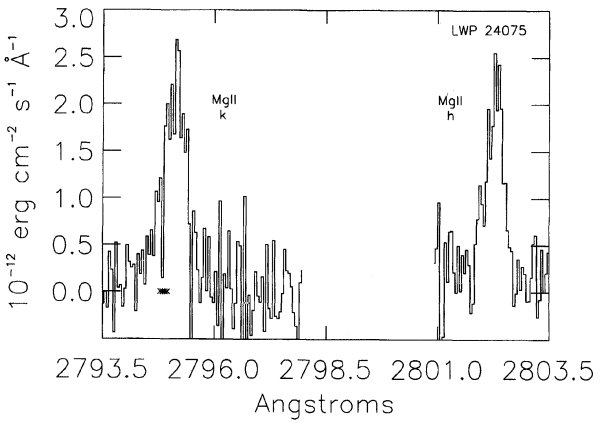

FIG. 5. Sample LWP spectrum for V815 Her. The spectrum (LWP24075) represents a typical or "quiescent" level.

© American Astronomical Society • Provided by the NASA Astrophysics Data System

1996AJ....111.1356D

TABLE 8. V815 Her Mg II fluxes.[a]

Phase	F_h		λ_c (+2800) Å		Width Å		F_k		λ_c (+2790) Å		Width Å	
0.26	9.3	2.2	2.941	2.330	0.491	0.280	10.1	1.3	5.729	5.145	0.370	UNR[b]
1.37	9.2	1.4	2.391	2.932	0.261	0.220	9.3	2.4	5.138	5.712	0.396	UNR[b]
1.90	9.6		3.216		0.390		13.2		6.080		0.567	
2.47	10.8		2.347		0.417		13.6		5.096		0.532	
3.02	11.8		3.298		0.486		16.0		6.112		0.656	
3.58	10.3		2.318		0.377		12.6		5.121		0.407	
4.13	12.3		3.254		0.574		13.3		6.042		0.571	
4.68[c]	7.6		2.652		0.905		14.4		5.518		0.968	
8.50	9.3		2.289		0.361		12.1		5.111		0.466	
Mean[d]	10.4				0.529		13.1				0.548	
σ	1.4				0.190		1.4				0.184	

Notes to TABLE 8

[a]Fluxes are in units of 10^{-13} ergs s^{-1} cm^{-2}.
[b]Line is unresolves.
[c]High radiation background, very noise spectrum.
[d]Two components were added for computing the mean and ς while UNR values wer not included.

TABLE 9. V815 Her integrated far-ultraviolet emission line fluxes.

Phase	O I 1305	C II 1335	Si IV 1396	Si IV 1402	C IV 1550	He II 1640	C I[b] 1658	Si II 1808	Si II 1817
0.30	0.49	1.51	0.82	0.30	2.92	1.67	0.65	0.52	0.94
1.41	0.31	1.52	0.63	0.33	2.87	1.72	1.10	—[c]	1.34
1.95	0.58	1.74	0.52	0.55	3.69	1.96	1.05	0.27	0.93
2.51	0.12	1.65	0.55	0.35	3.47	1.77	1.05	0.58	0.95
3.06	0.80	2.02	0.81	0.57	4.38	2.18	1.41	0.58	0.79
3.61	0.56	1.44	0.77	0.74	3.39	1.76	1.65	0.26	0.89
4.17	0.67	1.85	0.73	0.31	3.34	1.67	1.33	0.29	1.00
4.72	0.63	1.40	0.63	0.49	3.97	1.83	0.92	0.67	1.01
8.54	0.62	1.38	0.83	0.58	2.94	1.66	1.27	0.65	0.90
Mean	0.53	1.61	0.70	0.47	3.44	1.80	1.16	0.97	0.48
σ	0.18	0.21	0.12	0.15	0.48	0.15	0.27	0.15	0.18

Notes to TABLE 9

[a]Fluxes are in units of 10^{-13} ergs s^{-1} cm^{-2}.
[b]Blended line.
[c]Data were contaminated at the peak and could not be reliably fit. These values were excluded from mean and ς calculations.

spheric emission similar to that observed previously by Huenemoerder *et al.* (1990) and Dempsey *et al.* (1993a).

Data from BMO were obtained in August and October of 1992 and are also shown in Fig. 8. Due to their lower resolution, the IRT emission reversals are "smeared out" and the line core depth R_c is slightly elevated compared to the higher-resolution data. The September IRT data show a sharp increase near light minimum but there are few photometric points in this interval. In contrast, the August data appear essentially constant. Hα shows only erratic behavior and does not follow the IRT data as in the top of Fig. 8. Similar behavior is observed for the He I D_3 line and Hβ, which are not shown in Fig. 8. The Konkoly photometry are sparse in August but they are consistent with the light curves shown in Fig. 9.

Neff *et al.* (1995) describe a technique (based on the work of Huenemoerder & Ramsey 1987) in which the 7055 and 8860 Å absorption bands of the TiO molecule are used to determine the area and temperature of starspots on active stars. Both TiO bands become deeper with decreasing $T_{\rm eff}$, but with different temperature sensitivities. For spot temperatures between approximately 3000 and 3800 K, this technique can independently determine starspot temperature (from the ratio of the strengths of the two bands) and filling factor (from their absolute depths). The upper temperature limit for this technique is set by the temperature at which the 8860 Å band is first observable. For 3800 K$\leqslant T_{\rm spot} \leqslant$4000 K, only the 7055 Å band is detectable, but $T_{\rm spot}$ can still be determined by comparing TiO-band observations with contemporaneous photometry. Above $T_{\rm spot}$=4000 K, the 7055 Å band is too weak to be detectable from spots on active stars.

Figure 10 compares a 7055 Å region spectrum of IM Peg with a spectrum of χ Gem, an inactive K2 III star; the positions of the three strong TiO band heads in this region are marked. Because no absorption was measured in the 8860 Å band, the starspots that are producing the visual light variation must fill an insignificant fraction of the stellar surface or be warmer than 3800 K. Above $T_{\rm eff}$>4000 K, the intrinsic D_{7055} from a stellar photosphere declines rapidly to only a few percent (O'Neal *et al.* 1995) and we would detect excess 7055 Å band depth in the observed spectra only for very large spot filling factors.

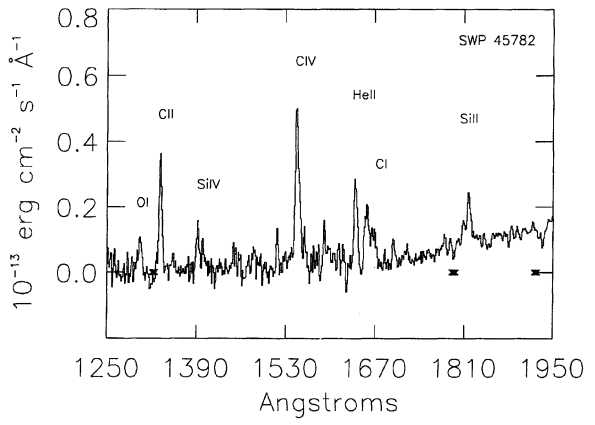

FIG. 6. Sample SWP spectrum for V815 Her. Several prominent lines are identified. The heavy "×"s along the bottom indicate camera reseau marks.

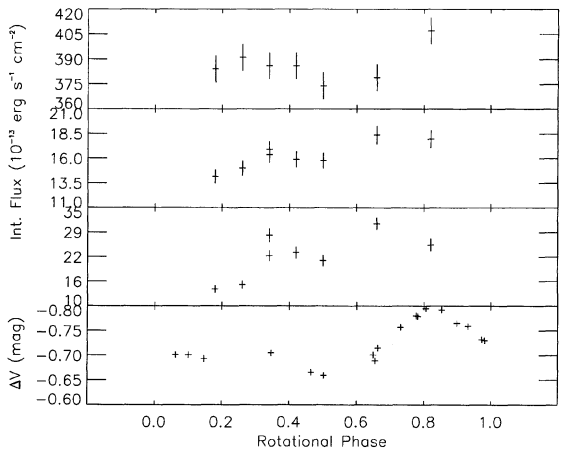

FIG. 7. *IUE* integrated Gaussian emission line fluxes versus phase V815 Her. From bottom to top: the visual light curve from Fig. 4, the summed Si IV and C IV line fluxes, representing the transition region, the combined Si II and C II flux, representing the chromosphere, and at the top the sum of the Mg II $h+k$ fluxes. The line flux measurements for all lines are given in Tables 8 and 9.

© American Astronomical Society • Provided by the NASA Astrophysics Data System

1996AJ....111.1356D

TABLE 10. IM Peg R_c measurements.[a]

HJD (+2440000)	Phase	Hα	8498Å	8542Å	8662Å
8836.8	0.89	0.77	0.83	0.73	0.73
8837.8	0.93	0.76	0.81	0.69	0.71
8839.8	0.01	0.77	0.81	0.71	0.74
8840.8	0.05	0.75	0.82	0.71	0.75
8841.8	0.09	0.74	0.82	0.70	0.74
8846.7	0.29	0.73	0.81	0.70	0.74
8854.7	0.61	0.75	0.81	0.68	0.71
8876.7	0.50	0.61	–	–	–
8877.8	0.55	0.63	–	–	–
8879.8	0.63	0.63	–	–	–
8880.8	0.67	0.58	–	–	–
8881.8	0.71	0.52	–	–	–
8887.8	0.96	0.59	0.76	0.67	–
8888.8	1.00	0.59	0.74	0.67	–
8889.8	0.03	0.61	0.77	0.67	–
8890.7	0.08	0.61	0.79	0.69	–
8891.7	0.12	0.63	0.78	0.67	–
8892.7	0.16	0.63	0.80	0.69	–
8893.7	0.20	0.67	0.80	0.69	–
8909.6	0.84	0.76	0.77	0.67	0.68
8917.6	0.17	0.68	–	–	–
8920.6	0.29	0.69	–	–	–
8921.6	0.33	0.70	–	–	–
8922.6	0.37	0.76	0.82	0.72	0.73
8923.6	0.41	0.76	0.84	0.76	0.76
8924.6	0.45	0.75	0.88	0.75	0.75
8934.6	0.86	0.75	0.81	0.69	0.72
Mean		0.68	0.80	0.70	0.73
σ		0.07	0.03	0.03	0.02

[a]Entries with "–" indicate no observation on that data for that wavelength.

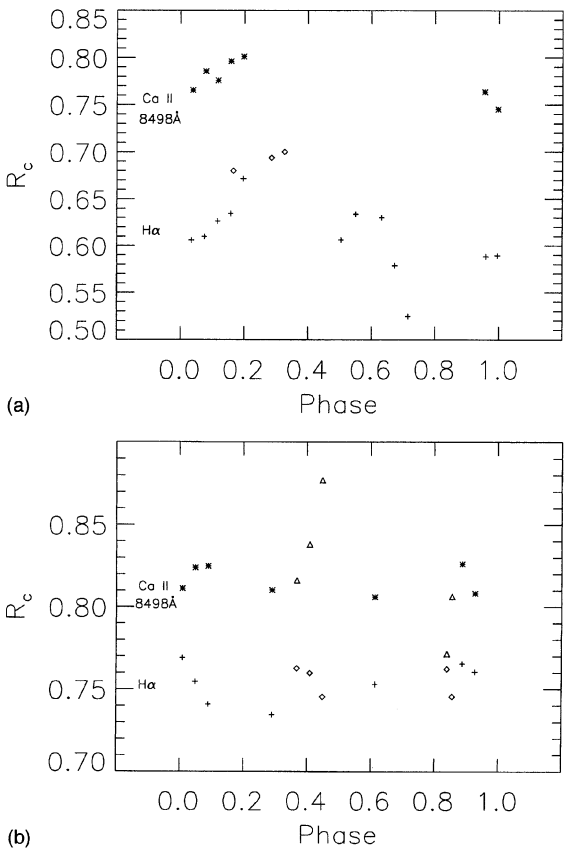

FIG. 8. (a) R_c for λ8498 (asterisks) and Hα (pluses and diamonds) for IM Peg. Higher R_c indicates increased line core emission. For Hα, pluses indicate KPNO and NSO data while the diamonds represent the RO data. Values of R_c for λ8542 are similar to those of λ8498 but with a smaller amplitude in the variation. (b) Data from BMO are shown in the bottom panel. Asterisks and triangles represent IRT data from August and September, respectively. R_c for Hα is designated by pluses and diamonds for the August and September data, respectively. Error bars are less than or equal to the size of the plotted symbols.

D_{7055}, the depth (relative to the normalized continuum) of the 7055 Å band measured by averaging the highest pixel intensity values in 5 Å wide band passes blueward and redward of the band head, varied from 0.019 at ϕ=0.51 to 0.031 at ϕ=0.67. Other observations were D_{7055}=0.027 at ϕ=0.55 and D_{7055}=0.020 at ϕ=0.63.

In order to calculate spot filling factors, we need to assume a spot temperature in the permissible range and a temperature for the nonspotted regions. A K2 giant star like IM Peg is cool enough to show a weak but measurable 1%–2.5% depth of the 7055 Å band even in the absence of spots. Assuming T_{spot}=3950 K and D_q, the absorption strength from the quiet photosphere, as 0.013 (equal to that found for a spectrum of χ Gem), we compute a maximum filling factor of 26%. If T_{spot}=4000 K, the maximum filling factor becomes 35%, while decreasing T_{spot} to 3900 K yields a 21% maximum filling factor. O'Neal *et al.* (1995) claim an uncertainty of ±0.005 in their bandhead depth measurements. Given the barely significant variation of 0.019–0.031 and the very limited phase coverage of the TiO observations, we would not expect to see a strong correlation between the TiO depth and the visual light curve.

Correlative Analysis (Dempsey *et al.* 1992) which uses cross-correlation to study profile distortions was applied to the KPNO data, but the detected asymmetries were questionable. To test the significance of these asymmetries, we calculated γ as defined in Dempsey *et al.* (1992). Of the five applicable observations, only one had $\gamma \approx 100$, while the rest were typically ≈40–80. In Dempsey *et al.* (1992), values of γ below 100 were considered nondetections. We note, however, that asymmetries as large as those seen in the 1989–1990 IM Peg observations (Dempsey *et al.* 1992) would easily have been detectable in our current dataset. Therefore, either no large spots in the photosphere were present at the time of observation, or the spots were distributed fairly uniformly in phase.

To model the light curve we use the photometric model of Strassmeier (1988, 1990) as described in Dempsey *et al.* (1992). In general, any number of square spots with any temperature may be used, but in practice 2–3 spots at a single temperature are usually adequate. The effects of such assumptions on the resulting trial-and-error fitted light curve are further discussed in Strassmeier (1994).

Originally, Dempsey *et al.* (1994) chose a cool spot temperature T_{spot} of 3520 K derived in the two-spot models of Poe & Eaton (1985) using *VRI* photometry. Poe & Eaton did not give a formal error for T_{spot} but stated that their method, in general, should have errors less than 200 K and in the case of IM Peg their temperature "should be realistic." Our con-

© American Astronomical Society • Provided by the NASA Astrophysics Data System

1996AJ....111.1356D

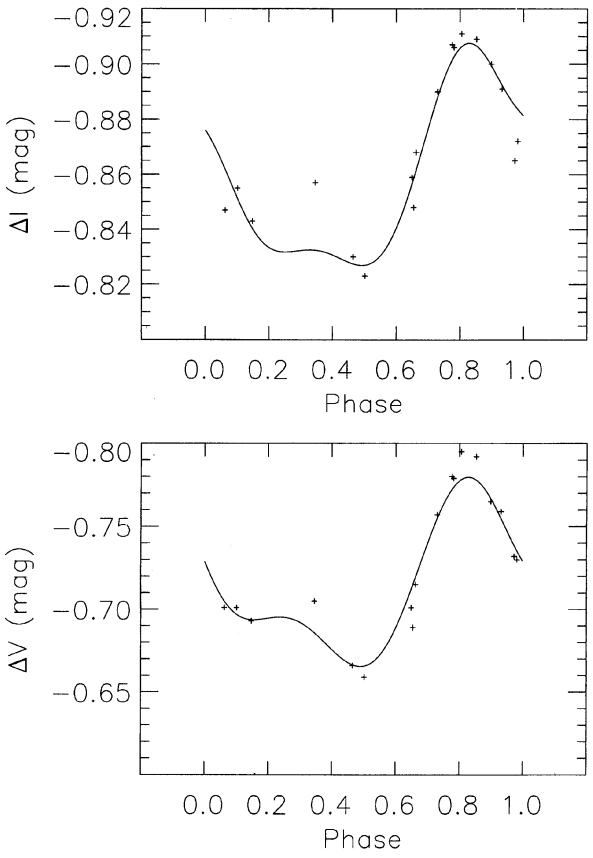

FIG. 9. Differential V-band (top) and I-band (bottom) light curves for IM Peg from fall of 1992. Increased brightness is towards the top. The solid line represents the spot model displayed in Fig. 11. The U, B, and R-band light curves were similar.

temporaneous photometry imply a T_{spot} of 3950±150 K in 1992. Because the TiO 8860 Å band would be detected if the spot were much cooler than this, we adopted a T_{spot} of 3950 K for the current modeling. It is not clear whether this really represents an increase in the spot temperature from the Poe & Eaton value. Using a warmer spot temperature requires

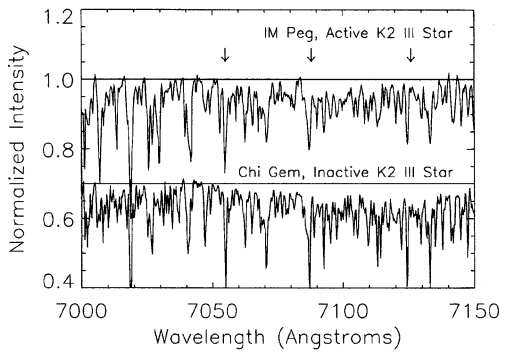

FIG. 10. A 7055 Å band spectrum of IM Peg compared with that of the inactive star χ Gem. Arrows indicate positions of the 7055, 7088, and 7126 Å bandheads of TiO. The lack of any excess TiO absorption on IM Peg implies that the spots are either relatively warm or cover an insignificant portion of the disk.

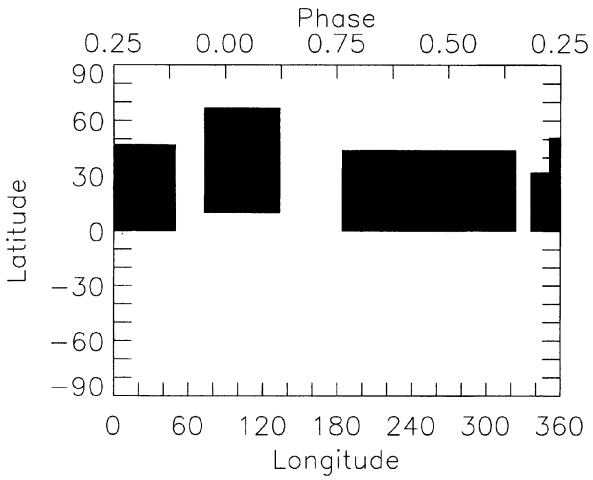

FIG. 11. Resulting starspot map for IM Peg. Dark shaded regions indicate a uniform T_{spot} of 3950 K.

larger areas to match the same light curve. The spot areas presented in Dempsey *et al.* (1994) would increase by approximately 20% using T_{spot} of 3950 K. The effective temperature of the primary was presumed to be 4400 K and V_0, the maximum brightness, was set at $5^m.60$, the brightest value observed in 17 years of photometric observation. Total spot area is directly related to V_0, and it is likely that the value of $5^m.60$ above does not represent a truly unspotted star but rather only the minimum spot coverage observed to date (the TiO results of Neff *et al.* 1995 imply that the active star II Peg was 35% spotted even at the epoch of maximum light; but see also Eaton *et al.* 1995). Little information is added to the modeling process by using the *UB* photometry (see, for example, Poe & Eaton 1985), so these were not directly used in the modeling. However, the resulting spot model does adequately reproduce the light curves in these bands. Limb darkening coefficients were taken to be 0.73, 0.53, and 0.42 for the V-, R-, and I bands, respectively. We adopted the Poe & Eaton value of 60° for the inclination.

From the September 1992 photometry we derive the map shown in Fig. 11. The resulting photometric model is shown in Fig. 9 as a solid line. The total projected spot area from the T_{spot}=3950 K photometric model is 27%, consistent with the $3900<T_{spot}<4050$ K and the maximum spot filling factor derived from the TiO bands. Changing T_{spot} 50 K alters the photometrically modeled area by less than 2%.

In order to determine if a real change in spot temperature had occurred between Poe & Eaton's modeling and ours, we refit their data using all the same parameters described above. We could not fit the data using T_{spot}=3950 K unless we altered other parameters such as V_0. We concur with Poe & Eaton (1985) that T_{spot}=3520 K yields the best fit to the earlier photometry. A slightly larger area of 9%, compared to Poe & Eaton's value of 7%, is derived in our modeling of their data but this is to be expected due to our using slightly different values for such key parameters as T_{eff} and V_0.

© American Astronomical Society • Provided by the NASA Astrophysics Data System

1996AJ....111.1356D

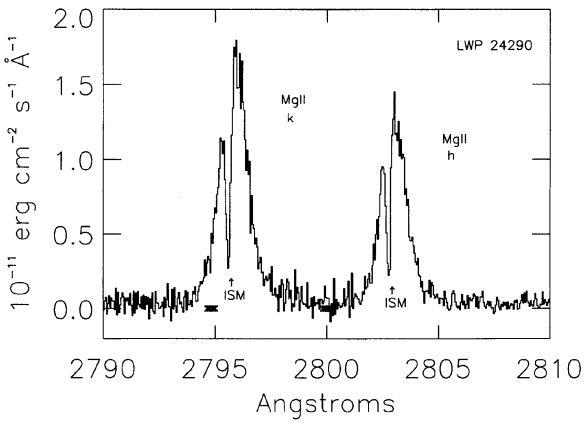

FIG. 12. Sample LWP spectrum for IM Peg.

4.2 Ultraviolet Data

Huenemoerder *et al.* (1990) first studied the UV variability of IM Peg using 10 *IUE* spectra obtained during the summers of 1985 and 1986. They found the UV fluxes to vary in phase with the Ca II IRT emission. Our *IUE* observations (see Table 4) were planned to cover one complete rotation in as short a time as possible. Figures 12 and 13 show typical LWP and SWP spectra of IM Peg, respectively. We fit the Mg II emission lines with a single Gaussian profile, along with a second Gaussian for the interstellar absorption. In all cases the single emission Gaussian fit the data well, so there is no evidence for emission from the secondary or for phase-dependent asymmetries caused by active regions. Line fluxes, corrected for the interstellar absorption, as a function of phase are given in Tables 11 and 12 and are shown in Fig. 14.

The Si III] and *C* III] line ratio can be used to estimate the electron density N_e, of the emitting plasma. Signal-to-noise is poor for these lines in our spectra, so the uncertainties in the ratio are large. From Keenan *et al.* (1987) we estimate that $N_e \approx 2.0 \pm 0.4 \times 10^{10}$ cm^{-3} assuming log $T_e = 4.7$ with the error estimated assuming 10% uncertainty in the fluxes. Different values in log T_e will change N_e by less than 5%.

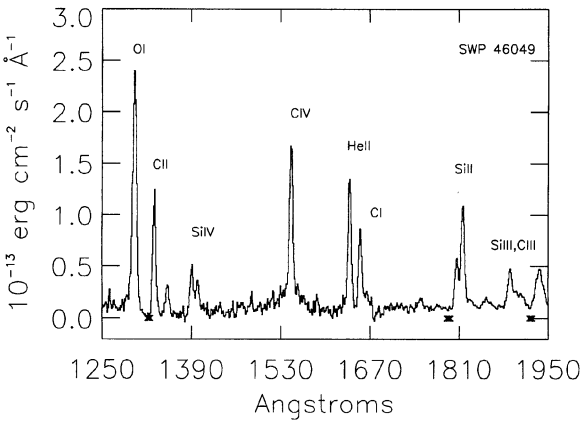

FIG. 13. Sample SWP spectrum for IM Peg. The heavy "×"s along the bottom indicate camera reseau marks.

TABLE 11. IM Peg Mg II fluxes.[a]

Phase	F_h	λ_c (+2800) Å	Width Å	F_k	λ_c (+2790) Å	Width Å
0.18	163	2.361	1.16	221	5.185	1.27
0.26	168	2.361	1.14	223	5.204	1.24
0.34	168	2.456	1.21	218	5.288	1.29
0.42	168	2.582	1.20	218	5.399	1.43
0.50	159	2.757	1.24	215	5.604	1.39
0.66	170	2.850	1.30	209	5.756	1.59
0.82	173	3.001	1.30	234	5.862	1.39
Mean	167		1.22	220		1.37
σ	5		0.06	8		0.12

[a]Fluxes are in units of 10ergs s^{-1}cm^{-2}.

5. DISCUSSION

We have discovered a possible third component in the V815 Her system. Since the only discernable change to the orbit has been to γ, the third component must have an orbital period on the order of decades. It is likely that the earliest Nadal *et al.* (1974) velocities, which were obtained 24 years prior to the bulk of their data, represent yet another value of γ. The paucity of data obtained over many years prevents us from more accurately characterizing the orbit of the third body.

The Hα and IRT lines of V815 Her showed significant variations in September 1992, but none that were clearly modulated with the rotational cycle. The visual brightness (Fig. 4) varied by $\geq$0.05 mag with a minimum around $\phi \sim 0.0$ and a maximum near $\phi \sim 0.5$. The ultraviolet emission lines (Fig. 7) varied, with the chromospheric and transition region (ultraviolet) emission varying crudely in antiphase with the (visual) photospheric brightness. This suggest that the spatial distribution of active regions is similar to the starspot distribution. This pattern, while often thought to be the standard picture of stellar activity, has only been seen on a few cases (e.g., Rodonò *et al.* 1987); the situation is generally more complex.

The emission reversal in the Hα line of IM Peg in 1992 September to October varied substantially (Fig. 8) and in clear antiphase to the photospheric brightness (Fig. 9). The phase coverage of the IRT lines and BMO data obtained during this interval was not adequate to determine if the

TABLE 12. IM Peg integrated far-ultraviolet emission line fluxes.

Phase	N V 1240	O I 1305	C II 1335	Si IV 1396	Si IV 1402	C IV 1550	He II 1640	C I[b] 1658	Si II 1808	Si II 1817	Si III] 1893	C III] 1909
0.18	5.08	15.98	4.02	2.25	2.17	9.80	4.70	4.02	3.06	7.07	2.75	1.68
0.26	5.74	17.50	5.07	2.98	2.10	10.27	8.36	5.07	2.96	6.97	5.44	1.83
0.34	8.46	16.63	5.93	4.32	4.65	18.98	8.94	5.93	3.65	7.31	3.02	1.84
0.34	5.89	14.99	4.25	3.16	4.30	15.28	8.13	4.25	4.78	7.35	4.09	3.47
0.42	6.54	16.68	5.14	3.79	2.92	16.94	7.05	5.14	3.23	7.54	4.92	2.33
0.50	6.40	17.10	4.80	3.49	2.93	15.13	6.35	4.80	3.61	7.36	5.13	1.92
0.66		[c]16.50	6.29	5.46	3.90	21.60	7.93	6.29	3.56	8.52	4.14	1.85
0.82	7.31	19.55	5.96	4.64	3.49	17.35		[c] 5.96	3.48	8.53	3.82	2.93
Mean	6.49	16.87	5.18	3.76	3.31	15.67	7.35	5.18	3.54	7.58	4.16	2.23
σ	1.03	1.23	0.76	0.96	0.88	3.78	1.44	0.76	0.53	0.57	0.90	0.60

Notes to TABLE 12

[aa]Fluxes are in units of 10^{-13} ergs s^{-1} cm^{-2}

[b]Blended line.

[c]Data could not be reliably fit. These values were exlcuded from mean and s calculations.

© American Astronomical Society • Provided by the NASA Astrophysics Data System

1996AJ....111.1356D

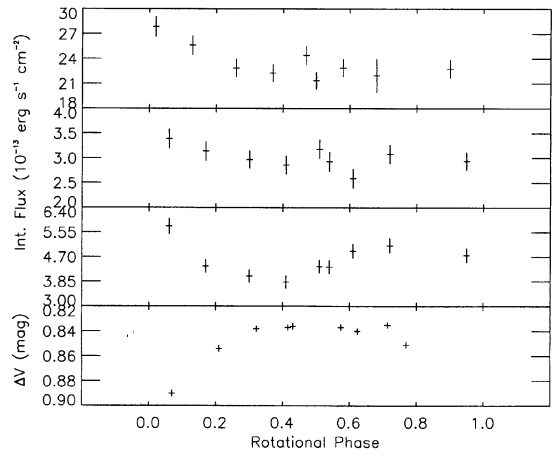

FIG. 14. *IUE* integrated Gaussian emission line fluxes vs phase for IM Peg. The panels are as in Fig. 7 except that the light curve is from Fig. 9. The line flux measurements for all lines are given in Tables 11 and 12.

variations were due to rotational modulation. The Mg II flux appears to correlate with the visual band variation (Fig. 14), but the Mg II variations are so small that they are also consistent with a constant sources (except at $\phi \sim 0.8$). The chromospheric and transition region lines show significant variations, but they do not vary smoothly with phase or correlate with the visual band variations.

While Huenemoerder *et al.* (1990) observed Hα to be essentially constant in IM Peg during the summers of 1985 and 1986, we observe a significant modulation in the Hα emission. Dempsey *et al.* (1994) tentatively identified a solar-like cycle on IM Peg based on 15 years of photometry. If valid, the Huenemoerder *et al.* (1990) Hα observations would roughly correspond to the spot minimum phase of the cycle, while those reported here occurred during spot maximum. This would suggest a possible change in the chromospheric network over the cycle. Long-term changes in Hα have also been observed for the RS CVn V711 Tauri (Dorren & Guinan 1990).

Further evidence for cycle related changes on IM Peg comes from the apparent change in T_{spot} over 15 years. Poe & Eaton (1985) measured their cooler spot temperature when IM Peg's spot area was at a minimum, while our data were obtained when spot area appeared to be at the highest levels yet observed (Dempsey *et al.* 1994). On the Sun we now know that there is an increase in emission from faculae at sunspot maximum, enough to more than compensate the flux due to the light lost from the spot (Foukal 1987; Foukal & Lean 1988). If applicable to IM Peg, our 1992 September observations occurred when facular emission would be strongest. Since it is likely that the large "spots" we observe photometrically are actually groups of smaller spots, such a brightening may diminish the effects of the spots yielding a warmer "mean" spot temperature. Although emission levels have been observed to change over stellar cycles (e.g., Dorren & Guinan 1990) this represents the first evidence of a change in spot temperature over a cycle period.

The authors thank B. W. Bopp for providing the Ritter Observatory spectra and J. Eaton for making his earlier data available to us. Research at CSC has been supported by NASA Grant No. NAS5-32616. RCD wishes to thank S. Osmer and M. Dew for help in preparing the manuscript. Research at Penn State University was partially funded through NASA Grant No. NAGW-2603. KO acknowledges the support of Hungarian Research Grant OTKA I/3-829. DO acknowledges support from the NASA Space Grant College Fellowship Program.

REFERENCES

Ayres, T. R., *et al.* 1995, ApJS, 96, 223
Bevington, P. R., 1969, Data Reduction and Error Analysis for the Physical Science (McGraw–Hill, New York)
Bohlin, R. C. 1986, ApJ, 308, 1001
Bohlin, R. C., & Grillmair, C. J. 1987, *IUE* NASA Newsletter, No. 33, 28
Bopp, B. W., & Dempsey, R. C. 1989, PASP, 101, 516
Bopp, B. W., Dempsey, R. C., & Maniak, S. 1988, ApJS, 68, 803
Bopp, B. W., Evans, D. S., & Lang, J. D. 1970, MNRAS, 147, 355
Bopp, B. W., Saar, S. H., Ambruster, C. W., Feldman, P., Dempsey, R. C., Allen, M., & Barden, S. 1989, ApJ, 339, 1059
Dempsey, R. C. 1991, Ph.D. thesis, University of Toledo, Toledo, OH
Dempsey R. C., Bopp, B. W., Strassmeier, K. G., Granados, A. F., Henry, G. W., & Hall, D. S. 1992, ApJ, 392, 187
Dempsey R. C., Bopp, B. W., Henry, G. W., & Hall, D. S. 1993a, ApJS, 86, 293
Dempsey, R. C., Bopp, B. W., Henry, G. W., & Hall, D. 1994, in Cool Stars, Stellar Systems, and the Sun, edited by J.-P. Caillault, ASP Conf. Ser., 64 (ASP, San Francisco), 393
Dempsey, R. C., Linsky, J. L, Fleming, T. A., & Schmitt, J. H. M. M. 1993b, ApJS, 86, 599
Dempsey, R. C., Linsky, J. L., Fleming, T. A., Schmitt, J. H. M. M., & Kürster, M. 1993c, in Physics of Solar and Stellar Coronae, edited by J. L. Linsky and S. Serio (Kluwer, Dordrecht), p. 361
Dempsey, R. C., Linsky, J. L, Schmitt, J. H. M. M., & Kürster, M. 1995, ApJS, in preparation
Dorren, J. D., & Guinan, E. F. 1990, ApJ, 348, 703
Doyle, J. G., Butler, C. J., Rodonò, M., Swank, J., & Fowles, W. 1989, A&A, 223, 219
Doyle, J. G., Butler, C. J., Byrne, P. B., Rodonò, M., Swank, J., & Fowles, W. 1989, A&A, 223, 219
Eaton, J. A., *et al.* 1983, A&SS, 89, 53
Eaton, J. A., Henry, G. W., & Fekel, F. C. 1995, ApJL, submitted
Foukal, P. 1987, J. Geophys. Res., 92, No D1, p. 801
Foukal, P., & Lean, J. 1988, ApJ, 328, 347
Hall, D. S. 1976, in Multiply Periodic Phenomena in Variable Stars, IAU Colloq. 29, edited by W. S. Fitch (Reidel, Dordrecht), p. 287
Hall, J. C., Fulton, E. E., Huenemoerder, D. P., Welty, A. D., & Neff, J. E. 1994, PASP, 106, 315
Huenemoerder, D., & Ramsey, L. 1987, ApJ, 319, 392
Huenemoerder, D., Ramsey, L., & Buzasi, D. 1990, ApJ, 350, 763
Keenan, F. P., Dufton, P. L., & Kingston, A. E. 1987, MNRAS, 225, 859
Landolt, A. U. 1983, AJ, 88, 439
Linsky, J. L., Neff, J. E., Brown, A., Gross, B. D., Simon, T., Andrews A. D., Rodonò, M., & Feldman, P. A. 1989, A&A, 211, 173
Menzies, J. W., Marang, F., Laing, J. D., Coulson, I. M., & Engelbrecht, C. A. 1991, MNRAS 248, 642

© American Astronomical Society • Provided by the NASA Astrophysics Data System

1996AJ....111.1356D

Montes, D., Fernández-Figueroa, M. J., De Castro, E., & Cornide, M. 1995, A&A 294, 165
Nadal, R., Pedoussaut, A., Ginestet, N., & Carquillat, J. M. 1974, A&A 37, 191
Neff, J. E. 1987, Ph.D. thesis, University of Colorado, Boulder
Neff, J. E., O'Neal, D., & Saar, S. H. 1995, ApJ (in press)
Neff, J. E., Walter, F. M., Rodonò, M., & Linsky, J. L. 1989, A&A 215, 79
O'Neal, D., Neff, J. E., & Saar, S. H. 1995, ApJ (submitted)
Poe, C. H., & Eaton, J., A. 1985, ApJ, 289, 644
Rodonò, M., *et al.* 1987, A&A, 176, 267
Strassmeier, K. G. 1988, A&SS, 140, 224
Strassmeier, K. G. 1990, ApJ, 348, 682
Strassmeier, K. G. 1994, A&A, 281, 395
Strassmeier, K. G., Hall, D. S., Fekel, F. C., & Scheck, M. 1993, A&AS, 100, 173

© American Astronomical Society • Provided by the NASA Astrophysics Data System